The Princeton Journal of Interdisciplinary Research
ISSN 3069-8200

Harnessing Riemannian Geometry to Predict Spotting

A Novel Model for Wildfire Embers

Arth Dalsania (author)[1]

[1]Newbury Park High School, Newbury Park, California, United States

Abstract

Operational wildfire spread models are crucial to informing the decisions made by wildfire responders. However, current models for wildfire spread through spotting (the transport of embers by wind) have limited accuracy, particularly in conditions of irregular terrain and wind. This study introduces a novel spotting prediction model that incorporates wind speed, relative humidity, and topography by employing differential geometry. The model uses a spacetime metric to account for meteorology and terrain and computes geodesic arc lengths between ignition and target points. A cutoff geodesic arc length threshold is set to be the median value based on training data from four California wildfires, occurring between 2000 and 2024, that included significant spotting activity. The model is then tested against the deterministic Albini spotting model, employed in operational tools such as FARSITE, and a control model based on Euclidean distance. Models are tested using data from the Sherpa and Thomas fire perimeters. The geodesic-based model equals or outperforms (within a 0.05 margin) the predictive accuracy of both the Albini model and control. A chi-squared test confirms that geodesic arc length is a better predictor of spotting events than Euclidean distance, specifically at further distances from the fire front. The results suggest that non-Euclidean effects on ember transport are nonnegligible, and geodesic methods can bolster spotting prediction.

Keywords: wildfire model, spotting, ember transport, pyro-convection, topography.

Introduction

Uncontrolled wildfires frequently cause harm to human populations and infrastructure, with adverse effects that span from public health issues to economic losses to human displacement. Effective wildfire modeling is essential for informing fire response strategies and operational decision-making by fire departments. Among the greatest challenges in wildfire modeling is spotting, the process of embers being lofted and transported by wind, igniting at a distance from the main fire front. Spotting is a non-local mechanism that is further complicated by fire-atmosphere interactions (pyro-convection), which generate turbulent and rapidly changing winds around an active fire. Spotting is especially difficult to predict in uneven terrain and under dry, windy conditions, conditions that are common in certain fire-prone regions such as California and Australia. Current deterministic models of spotting such as the Albini framework (1979) fall short in these scenarios, partly due to their limited ability to account for the effects of topographical complexity on ember trajectories.

This study introduces a novel spotting model that applies differential geometry to the wildfire environment. It is inspired by the stationary-action geodesic trajectories of photons in Einstein's theory of general relativity, which explains gravity as the curvature of spacetime. The novel spotting model formulates a spacetime metric from the first fundamental form, that depends on topography, wind speed, and relative humidity. Least-squares regression is used to fit a digital elevation model to a two-dimensional, second-degree polynomial. This allows the computation of the geodesic metric. The geodesic arc length (GAL) from an origin point to a potential ignition point is then calculated by solving a system of second-order ordinary differential equations derived from the geodesic equation in this metric. The solutions to the differential equations are implemented numerically using Python.

The model is trained using data from four California wildfires (2000-2024) in which spotting was a documented driver of spread. For each fire, three possible origin points and 20 likely spotting points are used to calculate both GAL and traditional Euclidean distance, yielding a dataset of 240 pairwise distances. For both metrics, the median distance defines a cutoff, and the probability of spotting is modeled with a Rayleigh distribution with the median as the scale parameter.

To evaluate performance, the GAL, Euclidean, and Albini models are tested on 120 points drawn from two wildfires (the Sherpa and Thomas fires) that were not used for training. A 5% spotting probability threshold is applied, and model performance is assessed using the Dice-Sorensen coefficient and F1 score. The GAL model demonstrates improved performance over the Euclidean baseline and achieves accuracy comparable to the Albini model, without requiring detailed fuel map inputs. Variational analysis (chi-squared importance) confirms that GAL is significantly more predictive of spotting than traditional Euclidean distance. These findings suggest that non-Euclidean effects play an important role in ember transport, and approaches that incorporate curvature can provide less computationally intensive alternatives to current models.

Methods

Novel GAL Model

In the new GAL model, the surface is treated like a smooth, two-dimensional Riemannian manifold embedded in three-dimensional space. The winds that drive spotting are assumed to be symmetric in the orientation of the surface relative to sea level. Although the pyro-convective winds are not parallel to the surface, the wind field is assumed to be independent of the ground incline. The Euclidean distance between two points on the two-dimensional map does not account for the features of the surface. The geodesic arc length between two points follows the tangent vector to the surface, and since winds are assumed to be oriented relative to the tangent, the geodesic distance is hypothesized to be a better metric of spotting probability than Euclidean distance.

Given a possible ember ignition point and a possible target point, the spacetime metric formulated for the GAL model was

$$ds^2 = (1 + (\frac{dz}{dx})^2)dx^2 + (1 + (\frac{dz}{dy})^2)dy^2 - v^2(1 - \gamma^2)dt^2 \quad (1)$$

The spatial components of this metric are derived from the first fundamental form, with $z(x, y)$ being the function that models the elevation at given coordinates. The metric defines the arc length ds. The metric incorporates the wind speed v and relative humidity γ as constants that are not functions of location or time. This is a spacetime metric, involving both space and time dimensions. It can be written as a diagonal 3-by-3, rank-2 tensor, $g_{\mu\nu}$, with the coefficients of (1) along the diagonals. Given two points, an origin point where an ember could emanate from, and a target point that the ember could ignite at, the change in time dt is given by the time interval that it is expected to take the ground spread of the fire to travel the Euclidean distance between the two points, $dt^2 = \frac{\Delta x^2+\Delta y^2}{R^2}$, where R is the rate of ground spread. This rate of ground spread is adjusted to be dependent on the relative humidity (see Comparison Models). The fitted elevation function takes the form

$$z(x, y) = \alpha x^2 + \beta y^2 + cx + dy + \eta \quad (2)$$

Least-squares regression is employed to fit this polynomial to sampled points from a digital elevation model. The regression algorithm entails finding the optimal values for the coefficients $\alpha, \beta, c, d,\ and\ \eta$. The geodesic path between the ignition and target points must obey the Riemann geodesic equation

$$\frac{d^2X^\lambda}{dp^2} + \Gamma^\lambda_{\mu\nu}\frac{dg^\mu}{dp}\frac{dg^\nu}{dp} = 0 \quad (3)$$

where X is the vector (x, y, t), and the Einstein summation convention is employed. The derivatives in (3) are taken with respect to p, which is the variable introduced to parametrize the geodesic curve. The Christoffel symbols $\Gamma^\lambda_{\mu\nu}$ in (3) are calculated from the spacetime metric $g_{\mu\nu}$ (the formula is omitted here for brevity). Once the geodesic path is calculated, the GAL is given by the integral

$$GAL = \int_{p_0}^{p_f} \sqrt{g_{\mu\nu}\frac{dx^\mu}{dp}\frac{dx^\nu}{dp}}\, dp \quad (4)$$

The geodesic equation then yields three, second-order ordinary differential equations that parametrize the geodesic between the origin point and target point, in terms of p. These equations are solved numerically, with the initial coordinates as the spatial coordinates of the origin point and $t = 0$. The derivatives are initialized by dividing the net change in position and time from origin to target by the range of the parameter. So, the initial vector "points directly at" the target point.

For each iteration, the second derivatives are calculated using the ordinary differential equation and first derivative. From the second derivative, the first derivative is updated as $x' \to x' + x''\,\delta p$. The coordinate x itself is updated by a correction of $\frac{1}{2}\frac{dx^2}{dp^2}\delta p^2 + \frac{dx}{dp}\delta p$. Here, δp is the small increment in the p-value in each iteration. This is a second-order implementation of Euler's method for approximating ordinary differential equations. The y and t coordinates are calculated similarly. At each iteration, the GAL is updated by an increase by $\delta p\sqrt{g_{\mu\nu}\frac{dx^\mu}{dp}\frac{dx^\nu}{dp}}$. This is a Riemann sum approximation of the arc length integral. The GAL is used to calculate the probability tail (see Probability Distribution) for a new origin-target pair, to classify it as a predicted spotting event or not.

Comparison Models

The novel GAL model is compared to the spotting model that is currently the most popular for predicting spotting events in operational wildfire modeling, the Albini model. Since the tested wildfires occurred on primarily mixed chaparral fuel landscapes in southern California, the Albini model is implemented with that fuel type. The standard available energy for chaparral fuel is around $8914\frac{kJ}{kg}$ (Sun et al., 2005), and the fuel bulk density (in megagrams per hectare) is about $20\frac{Mg}{ha}$ (Regelbrugge et al.). The fireline intensity, the energy evolved by the fire per unit time, is calculated using Byram's Law,

$$fireline\ intensity = (fuel\ energy) \times (rate\ of\ spread) \quad (5)$$

The chaparral fuel height is taken to be approximately 2 meters (Zhou et al. 2005). The rate of ground spread is estimated as $0.36\frac{m}{s}$ in a relative humidity of 0.42, based on the data collected by Stephens et al. from prescribed chaparral wildfires in northern California in 2008. The rate of spread is adjusted based on relative humidity based on the data collected by Awad et al. (2020) as

$$R(\gamma) = R(0.42) \times [\frac{0.42}{\gamma}]^{0.2} \quad (6)$$

Here, the rate of spread R is approximated as a function of relative humidity γ. From the fireline intensity, Albini's 1983 semi-empirical formulas for plume height and maximum spotting distance on flat ground are used. They are omitted here for the sake of brevity. The formula presented there for mountainous terrain cannot be used since the tested origin-target pairs do not conform to the midslope-valley-ridgetop classification employed by Albini and Chase (1981). That classification system cannot be applied between two points on an arbitrary irregular surface given a digital elevation map.

The GAL model is juxtaposed with both the Albini model and a Euclidean version, which involves the same statistical training method and probability distribution (see Probability Distribution). The Euclidean model replaces the GAL as a metric with the two-dimensional Euclidean distance $\sqrt{\Delta x^2 + \Delta y^2}$. This control is used to assess the contribution of the geodesic and spacetime aspects of the GAL model to its accuracy.

ISSN 3069-8200

Probability Distribution

The Rayleigh probability distribution has been found to be the most accurate for modeling spotting probability (Wang, 2011).

Figure 1

Rayleigh Probability Density Function with Mode σ = 1

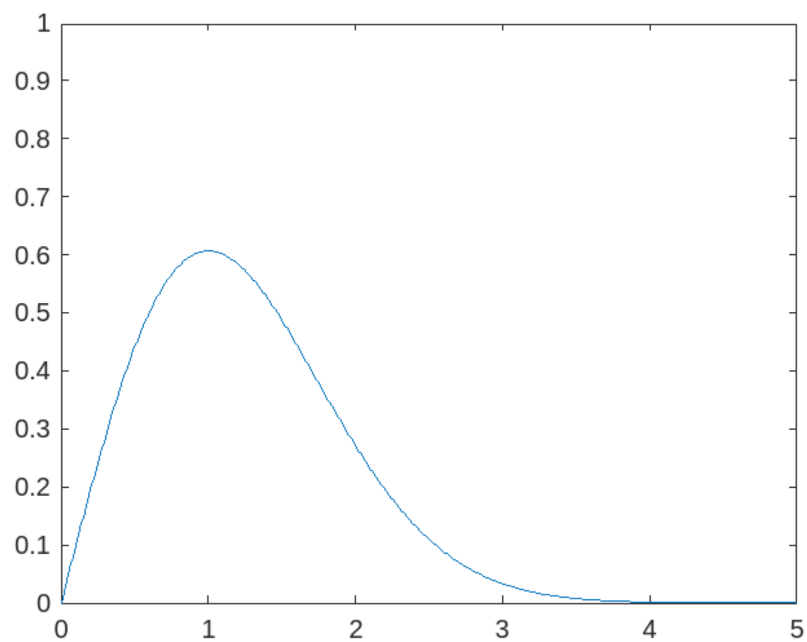

Each model that is tested has a metric that determines spotting prediction. This is the maximum spotting distance for the Albini model, the median GAL from the training data for the GAL model, and the median Euclidean distance from the training data for the Euclidean model. The medians are used because an equal number of spotted and non-spotted points will be in the training dataset, so the median is expected to be the optimal binary cutoff. These metrics are used as the median scale parameter of a Rayleigh probability distribution, an example of which is shown in Figure 1. The right tail cumulative distribution function

$$f(X \geq x) = e^{-x^2/(2\sigma)^2} \quad (7)$$

where σ is the mode, related to the median M by

$$M = \sigma\sqrt{2\ ln2} \quad (8)$$

If the right probability tail of a new origin-target pair is greater than the minimum probability cutoff (set to 0.05, see Methods), then the given model predicts that spotting will occur.

Wildfire Data

The accuracies of the three models are tested based on wildfire perimeter and meteorological data from 2 wildfires in southern California between 2000 and 2024. Before testing, the GAL model and a Euclidean model are trained on data from 4 of those wildfires, to obtain median metrics.

Table 1

Windspeed, Relative Humidity, and Metadata for the 4 Training and 2 Testing Wildfires

Fire	Use	Area ($\mathbf{10^7\ m^2}$)	Alarm Date	RAWS	Wind Speed ($\frac{m}{s}$)	Relative Humidity
Sherpa	Tst	3.02	6/14/2016	Refugio	9.8	0.69
Alisal	Tr	6.86	10/10/2021	Gaviota	8.2	0.60
Thomas	Tst	114	12/3/2017	Montecito 2	1.6	0.60
Gap	Tr	3.86	6/30/2008	Los Prietos	0.8	0.50

Jesusita	Tr	3.53	5/4/2009	Montecito 1	2.9	0.53
Whittier	Tr	7.45	7/7/2017	Refugio	6.4	0.26

Note. The wildfire data is sourced from IRWIN (Integrated Reporting of Wildfire Information).

The label Tr indicates that the fire was used to generate model training data for this study, while the label Tst indicates the fire was used to generate data points that the models were tested on. The area refers to the total burned area, and both wind speed and relative humidity are daily averages.

The wildfire perimeters are obtained from the CAL FIRE CalFrap dataset projected onto the coordinate system EPSG 3857. The wind speed and relative humidity are obtained from the nearest Remote Automated Weather Station (RAWS) that has meteorological data from the alarm date of that wildfire, as shown in Table 1. They are trained on a total of 240 data points and tested on another 120 points. Each data point is an origin-target point combination. For each of the wildfires, the Shuttle Radar Topography Mission (SRTM) 30-meter digital elevation model is used to sample 10 points that represent the features of the topography that the fire occurs on. These points are entered into the least-squares polynomial fitting algorithm, yielding an elevation function $z(x, y)$ in the form of (2). An example of the selection of representative points for elevation function fitting is shown in Figure 2.

For each wildfire, 3 different origin points, not necessarily the same as the topography sampling points), all within the observed fire perimeters, are sampled. These origin points are not the same as any of the topography sampling points, to avoid overfitting bias in the results. After the origin points are selected for a given wildfire, 20 target points are sampled. This includes 10 points which are within the final perimeters (spotting did occur) and 10 of which are not within the final perimeters (spotting did not occur). The medians can be used as a binary cutoff because the number of spotted and non-spotted training data points are equal (see Probability Distribution).

Figure 2

Elevation Point Sampling for the Sherpa Fire Landscape

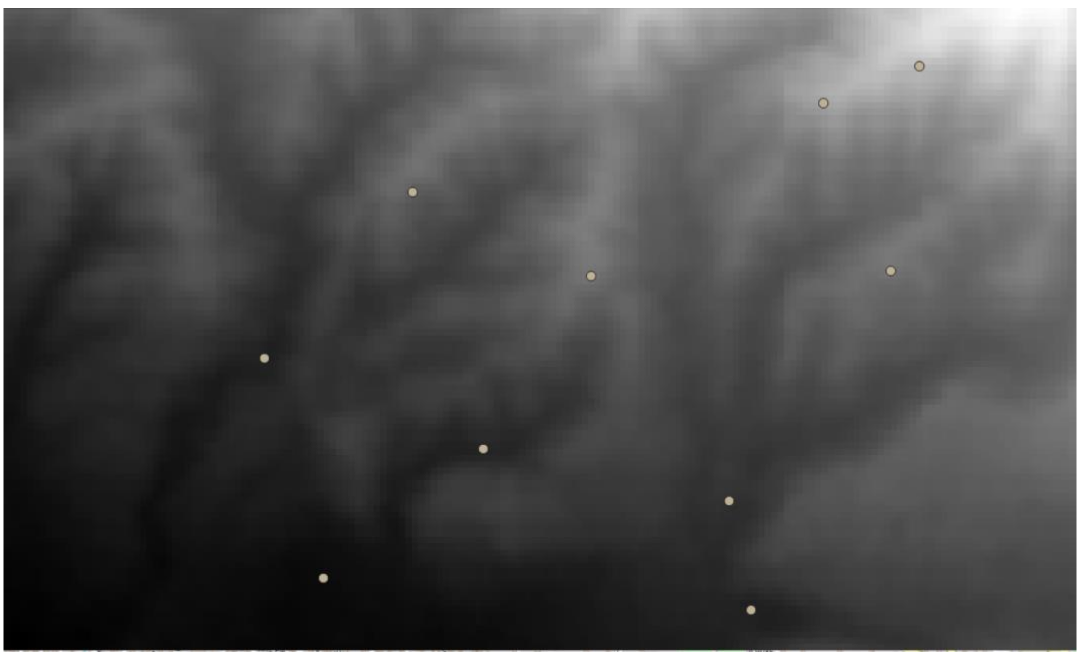

Note. Shuttle Radar Topography Mission 30-meter digital elevation model is used to sample 10 points representatives of the wildfire topography.

For each origin-target pair in the training dataset, the GAL and Euclidean distance are calculated and recorded, in addition to the spotting value of that target point. The spotting value is 0 if spotting did not occur and 1 if spotting did occur. The GAL is calculated using the numerical approximation algorithm (with 100 iterations). The algorithm is implemented with a Python script. For the 2 testing wildfires, the spotting value prediction, whether a given model predicts that spotting will occur, for each of the three models is recorded. The actual spotting value is also recorded.

Controls and Assumptions

It is assumed that the effects of fire response and fire spread along the ground do not change spotting between the chosen origin and target points. An example of the selection of target points is shown in Figure 3. It is also assumed that the exact choice of origin point in a small region within the fire perimeter does not affect the spotting probability. Areas along the fire perimeter chosen for training and testing were selected due to their outcropping shape, indicating that it is likely that spotting occurred along those boundaries. The vegetation fuel type, mixed chaparral, was controlled in the wildfires and areas chosen. Wildfires were also chosen such that for each fire, there have been a maximum of three *other* overlapping fires in interest between 2000 to 2024. Fuel maturity is controlled to the extent possible by this selection criterion.

Figure 3

Spotting Point Sampling for the Whittier Fire perimeter

Note. For each wildfire, 20 points are sampled. The outcropping shape of the boundary in the proximity of the sampled regions indicates that spotting was the likely primary driver of fire spread there.

Results

The results indicate that the GAL model consistently outperforms the Euclidean model and has comparable accuracy to the Albini model. The median Euclidean distance was found to be 600.6 meters, and the median GAL was found to be 5444 meters. The accuracy of a wildfire model is commonly evaluated using the Dice-Sorensen coefficient (DSC), which measures the relative intersection of two sets (X and Y), given by

$$DSC(X,Y) = \frac{2|X \cap Y|}{|X|+|Y|} \quad (9)$$

where $|S|$ indicates the order, or cardinality, of set S. Here, the Dice-Sorensen coefficient between the actual data and a given model's predictions is used. Since it is assumed that the sampled origin-target points are representative of the topography of the areas tested, the discrete Dice-Sorensen coefficient from the sampled points is expected to adequately approximate the exact, areal Dice-Sorensen coefficient. The Dice-Sorensen coefficients of the tested models are displayed in Figure 4. The Albini, Euclidean, and GAL algorithms are compared as predictive models by the F1 score. The F1 score incorporates both the precision and recall of a model. Precision refers to the ability to minimize false positives, and recall refers to the ability to identify true positives. It is given by

$$F1 = \frac{TP}{TP + \frac{1}{2}(FP + FN)} \quad (10)$$

where TP is the number of true positives, FP is the number of false positives, and FN is the number of false negatives. The F1 scores of the tested models are displayed in Figure 5. The distributions of Euclidean distances to points where spotting was predicted to occur by each model are analyzed, as displayed in Figures 6 and 7. These distributions are compared to the distribution of distances to points where spotting did occur.

Figure 4

Dice-Sorensen Coefficients for Albini, Euclidean, and Geodesic (GAL) Models

The Princeton Journal of Interdisciplinary Research
ISSN 3069-8200

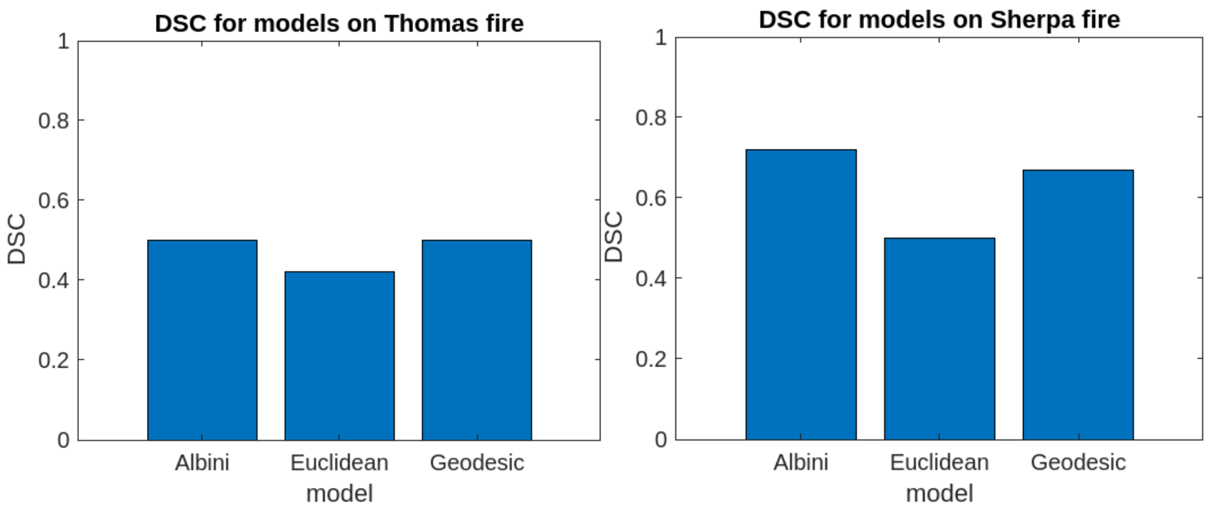

Figure 5

F1 Scores for Albini, Euclidean, and Geodesic (GAL) Models

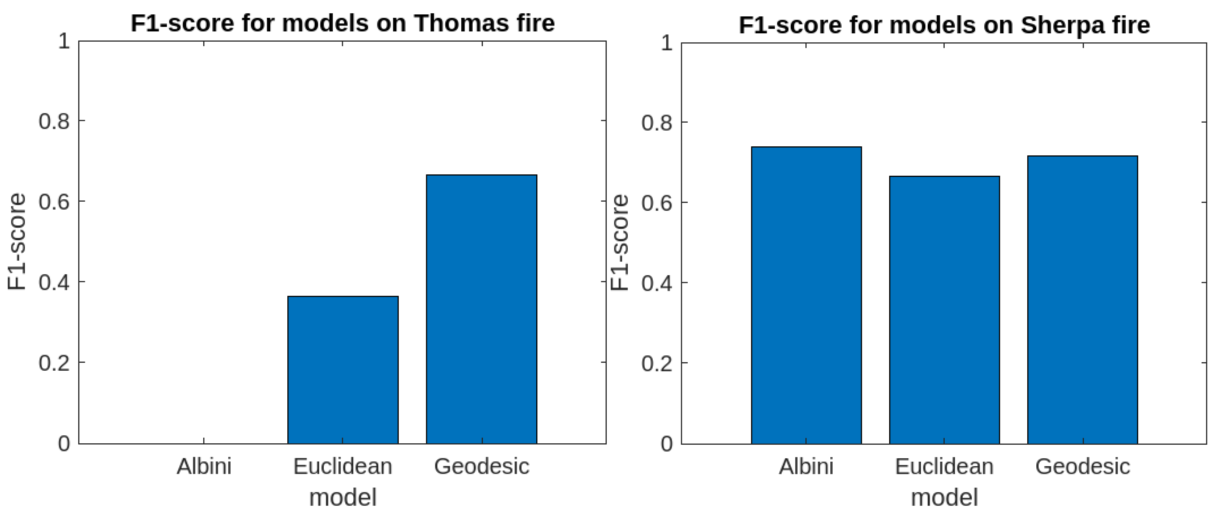

Note. Notably, the Albini model did not predict any spotting for the Thomas fire.

Figure 6

Distributions of Predicted and Actual Spotted Points for the Thomas Fire

Control Thomas Fire Spotting Predictions

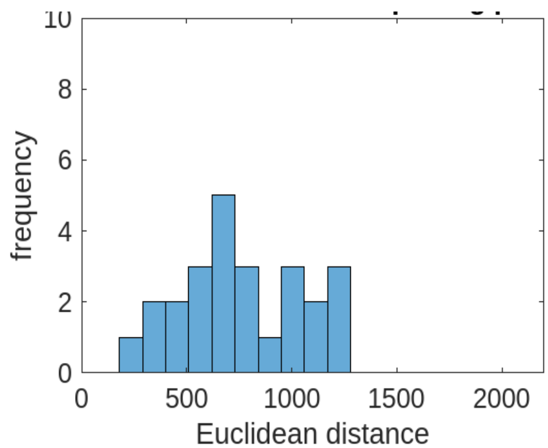

GAL Model Thomas Fire Spotting Predictions

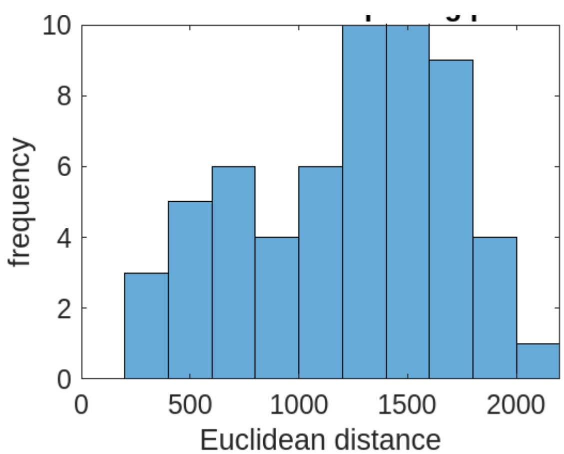

Actual Thomas Fire Spotting Events

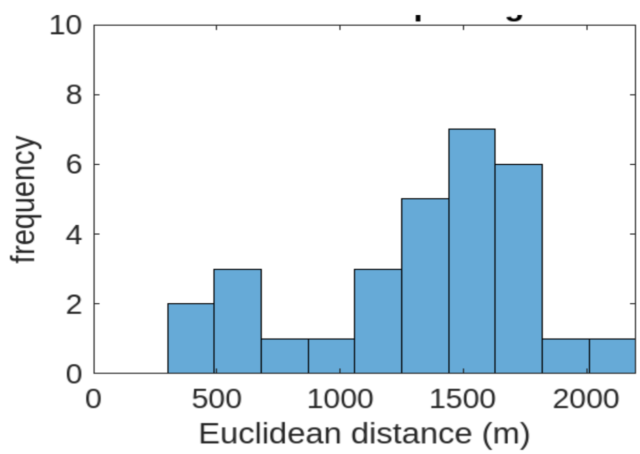

Note. No histogram for the Albini model tested on the Thomas fire is present, because the Albini model did not predict any spotting events for the Thomas fire data points.

The Princeton Journal of Interdisciplinary Research
ISSN 3069-8200

Figure 7

Distributions of Predicted and Actual Spotted Points for the Sherpa Fire

Albini Model Sherpa Fire Spotting Predictions

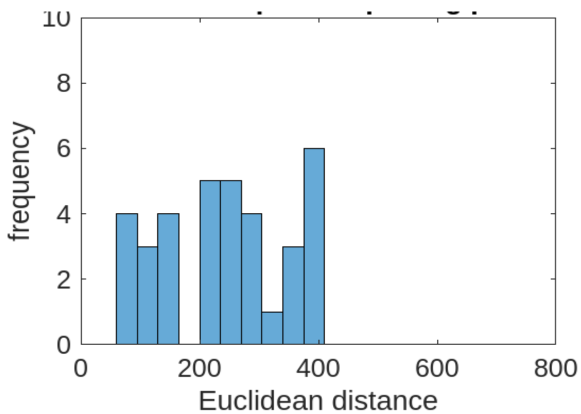

Control Sherpa Fire Spotting Predictions

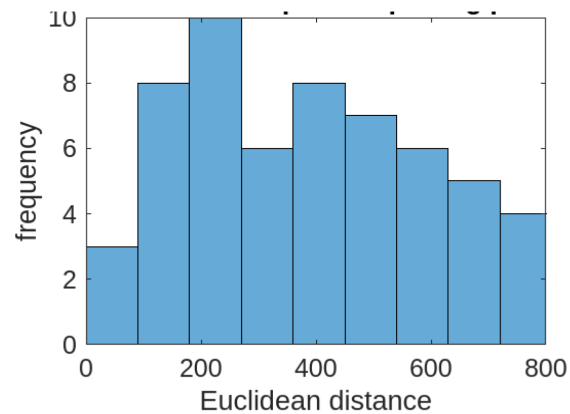

GAL Model Sherpa Fire Spotting Predictions

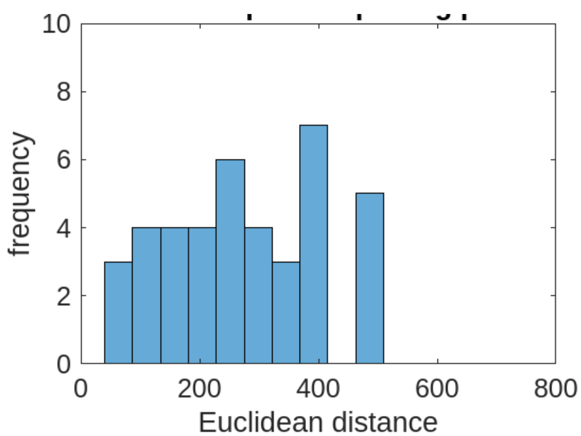

Actual Sherpa Fire Spotting Events

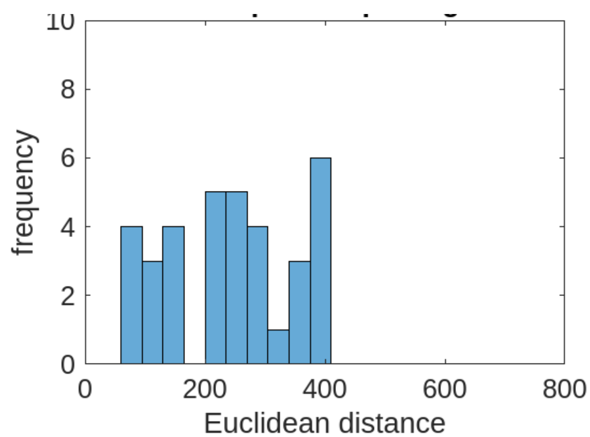

The distance distribution histograms indicate that the GAL model is more accurate than the Euclidean model at larger distances. The accuracy of the Albini model for the Sherpa fire is greater than the GAL model, but both bear similar distributions, while the Euclidean model significantly overestimates spotting at larger distances.

The Princeton Journal of Interdisciplinary Research
ISSN 3069-8200

The chi-squared test is used to assess whether the Euclidean distance or GAL is a better predictor of spotting events in the data tested. The chi-squared importance scores of the 4 most predictive factors are displayed in Figure 8. The test indicates that GAL is about 27.8% more predictive than the Euclidean distance, based on chi-squared importance score.

Figure 8

Chi-Squared Importance Scores for Target Point Coordinates, Euclidean Distance, and GAL

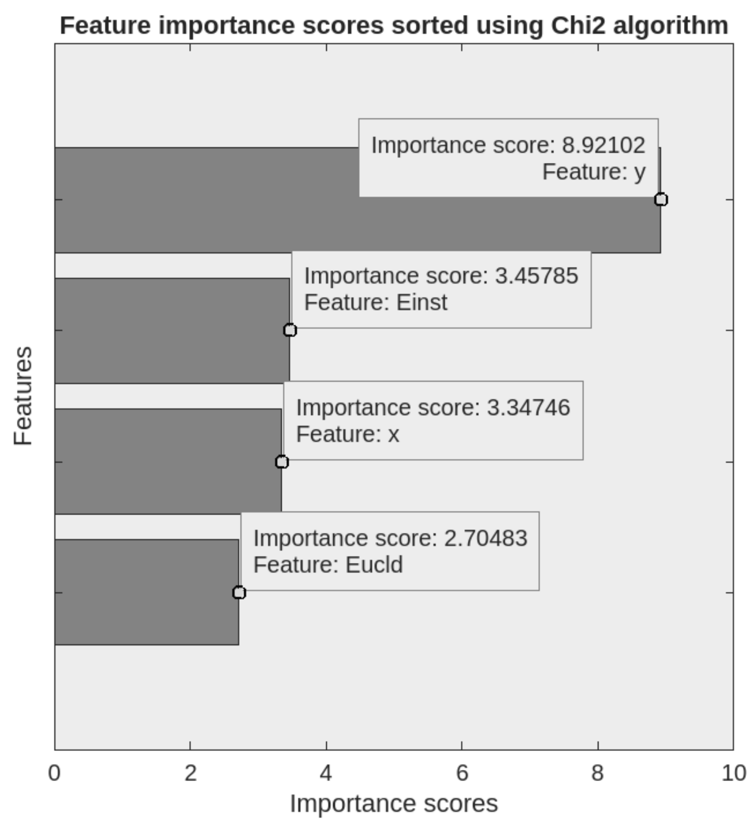

Note. The factors tested are the coordinates *x* and *y* of the target point, Euclidean distance (Eucld), and GAL (Einst). A kernel-based test was conducted using the fine Gaussian kernel. The *x* and *y* importance scores are an artifact of the orientation of the wildfire boundaries that were sampled.

The results indicate that the GAL model has comparable accuracy to the current Albini model. The Albini model performed better for the Sherpa fire, but the difference between the models was within 0.05. There is a notable exception in the case of the Thomas fire, in which the Albini model predicted no spotting for any of the tested points, corresponding to a Dice-Sorenson coefficient of 0.5 and F1 score of 0. The GAL model consistently outperformed the Euclidean model for both tested fires. The chi-squared test demonstrates that the GAL is a stronger predictor of spotting events than Euclidean distance.

Discussion

The findings of the study partially confirm the hypothesized improvements of the GAL model. The results show that the GAL model is consistently more accurate in predicting spotting than the Euclidean control model, and that GAL is a better predictor of spotting events than traditional Euclidean distance. This is especially supported at larger distances from the origin point, which corroborates the hypothesis that GAL adheres more closely to ember-transporting winds over irregular topography than Euclidean distance. The results indicate that the effects of non-flat landscapes are significant in wildfire ember spread, and that future models can gain improved accuracy by incorporating differential geometry to account for surface curvature.

In general, the GAL model closely matches and does not exceed the accuracy of the Albini model; there is a notable exception in the case of the Thomas fire, in which the Albini model predicted that no spotting would occur. This exemplifies the inaccuracy of the Albini model in the case of irregular terrain, and the GAL model can address these errors. The GAL model has the benefit of not requiring fuel landscape data, which the Albini model requires. Fuel surveys for regions at risk of wildfires are often costly and time-intensive, and fuel-informed wildfire models are likely to need more computational power and data. For these reasons, the prospect of an operational spotting model that achieves comparable accuracy to current models without needing fuel data offers a practical advantage for fire departments.

The findings of this study should be replicated for wildfire data from other regions of the United States and the world, although the extent to which spotting is a factor in wildfire spread may vary depending on fuel types, climate, and topography. Training and testing the GAL model on more data, as well as employing machine learning methods to separate spotting and non-spotting points, different from the median binary cutoff used in this study, could potentially increase the model's accuracy.

A drawback of the methodology used in this study is the assumption that the origin-target pairs that are sampled from within the fire perimeters are the result of spotting, based on firefighter observations and the shape of the fire perimeter. A possible solution to the problem of rigorously distinguishing spotting from non-spotting is to train a machine learning model such as a convolutional neural network to determine whether a fire perimeter is the result of spotting or ground spread.

Future research could involve the use of more advanced machine learning models, such as convolutional neural networks (CNNs), integrated with the GAL algorithm to predict spotting events based on spatial signatures in satellite imagery. Modeling wind velocity as a vector field that varies over space and time can also enhance accuracy by accounting for fire-atmosphere coupling, although it would also increase computational burden. The polynomial approximation

ISSN 3069-8200

of mountainous terrain breaks down at larger distances, so alternate methods of modeling the topography with a continuously differentiable function can also be employed in future studies.

Spotting models should be used in conjunction with ground spread algorithms to create accurate, comprehensive, and efficient operational wildfire models. Better models will optimize the reliability and efficacy of evacuation orders and firefighter deployment, as well as inform wildfire risk prediction and prevention measures.

References

Albini, F. (1979). Spot Fire Distance From Burning Trees–a Predictive Model. *USDA Forest Service General Technical Report.*

Albini, F. (1983). Potential Spotting Distance from Wind-Driven Surface Fires. *United States Department of Agriculture Forest Service.*

Awad, C. et al. (2020). Fuel Moisture Content Threshold Leading to Fire Extinction Under Marginal Conditions. *Fire Safety Journal Vol. 118*.

Billmire, M. (2014). Santa Ana winds and predictors of wildfire progression in southern California. *International Journal of Wildland Fire.*

Boychuk, D. et al. (2009). A stochastic forest fire growth model. *Environmental and Ecological Statistics.*

Brown, J. (1982). Bulk Densities of Nonuniform Surface Fuels and Their Application. Bulk Densities of Nonuniform Surface Fuels and Their Application to Fire Modeling. *Forest Science 27(4):667-683.*

Butler, B. et al. (2004). A radiation-driven model for crown fire spread. *NRC Research Press.*

Cardil A. et al. (2023). Performance of operational fire spread models in California. *International Journal of Wildland Fire.*

Chase, C. (1981). Spot Fire Distance Equations for Pocket Calculators. *United States Department of Agriculture Forest Service.*

Chase, C. (1984). Spotting Distance from Wind-Driven Surface Fires–Extensions of Equations for Pocket Calculators. *United States Department of Agriculture Forest Service.*

Conard, S. et al (1993). On Estimating Fuel Characteristics in California Chaparral. *12th*

Conference on Fire and Forest Meteorology.

Cova, G. et al. (2023). The outsized role of California's largest wildfires in changing forest burn patterns and coarsening ecosystem scale. *Forest Ecology and Management.*

Cruz, A. et al (2013). Limitations on the accuracy of model predictions of wildland fire behaviour: A state-of-the-knowledge overview. *Forestry Chronicle.*

Forest Fire Using VIIRS-Based Data and Machine Learning. MDPI Remote Sensing.

Green, L. (1982). Prescribed Burning in the California Mediterranean Ecosystem. *U.S. Department of Agriculture.*

Javaloyes, M. et al. (2021). A General Model for Wildfire Propagation with Wind and Slope. https://arxiv.org/abs/2110.03364

Javaloyes, M. et al. (2021). Applications of Cone Structures to the Anisotropic Rheonomic Huygens' Principle. arXiv:2010.11990v3.

Lopez-De-Castro, M. et al. (2024). Fire-spotting modelling in operational wildfire simulators based on Cellular Automata: A comparison study. *Agricultural and Forest Meteorology.*

Mandel, J. et al. (2011). Coupled atmosphere-wildland fire modeling with WRF 3.3 and SFIRE 2011. *Geoscientific Model Development.*

Martin, J. et al. (2016) The Spotting Distribution of Wildfires. *MDPI Applied Sciences.*

Mendez, A. et al. (2022). Quantifying rare events in spotting: How far do wildfires spread? https://www.sciencedirect.com/science/article/pii/S0379711222001084.

Patton, C. et al. (2021). New Biomass Estimates for Chaparral-Dominated Southern California Landscapes. *MDPI Remote Sensing.*

Radke, D. et al. (2019). FireCast: Leveraging Deep Learning to Predict Wildfire Spread.

Proceedings of the Twenty-Eighth International Joint Conference on Artificial Intelligence.

Rothermel, R. et al. (1973). Predicting Changes in Chaparral Flammability. *Journal of Forestry.*

Rothermel, R. (1972). A Mathematical model for predicting fire spread in wildland fuels. *USDA Forest Service.*

Regelbrugge J. et al. Biomass and Fuel Characteristics of Chaparral in Southern California. *Fire in California Ecosystems: Integrating Ecology, Prevention, and Management.*

Shaddy, B. et al. (2024). Generative Algorithms for Fusion of Physics-Based Wildfire Spread Models with Satellite Data for Initializing Wildfire Forecasts. *Artificial Intelligence for the Earth Systems.*

Son, M. et al. (2024). Development of an Algorithm for Assessing the Scope of Large Forest Fire Using VIIRS-Based Data and Machine Learning. *MDPI Remote Sensing*.

Stephens, S. et al. (2008). Measuring the rate of spread of Chaparral prescribed fires in northern California. *Fire Ecology Vol. 4, No. 1.*

Storey, M. et al (2020). Drivers of long-distance spotting during wildfires in south-eastern Australia. *International Journal of Wildland Fire.*

Sun, L. et al. (2005). Numerical Simulation of Live Chaparral Fire Behavior Using FIRETEC. *Scholarly Commons.*

Truccia, A. et al. (2018). Surrogate-based global sensitivity analysis for turbulence and fire-spotting effects in regional-scale wildland fire modeling. arXiv:1809.05430v1

Wang, H. (2011). Analysis on Downwind Distribution of Firebrands Sourced from a Wildland Fire. *Fire Technology Vol. 47*.

Zigner, K. et al. Evaluating the Ability of FARSITE to Simulate Wildfires Influenced by

Extreme, Downslope Winds in Santa Barbara, California (2020). *MDPI Fire.*

Supplemental Information

Link to a GitHub repository with the Python code used to fit a polynomial function to digital elevation data points, and the code used to implement each of the three tested models.

Acknowledgements

This research project would not have been possible without the operational wildfire modeling insight and field knowledge that the author received from Mr. Brian Heath, Ventura County Fire Department Fire Captain.